Measurement of the Σ^- Charge Radius by Σ^-–Electron Elastic Scattering

The SELEX Collaboration

I. Eschrich [i,1,2], H. Krüger [i,3], J. Simon [i,4], K. Vorwalter [i,5], G. Alkhazov [k], A.G. Atamantchouk [k,6], M.Y. Balatz [h,6], N.F. Bondar [k], P.S. Cooper [e], L.J. Dauwe [q], G.V. Davidenko [h], U. Dersch [i,7], G. Dirkes [i,8], A.G. Dolgolenko [h], G.B. Dzyubenko [h], R. Edelstein [c], L. Emediato [s], A.M.F. Endler [d], J. Engelfried [m,e], C.O. Escobar [s,9], A.V. Evdokimov [h], I.S. Filimonov [j,6], F.G. Garcia [s,e], M. Gaspero [r], I. Giller [ℓ], V.L. Golovtsov [k], P. Gouffon [s], E. Gülmez [b], He Kangling [g], M. Iori [r], S.Y. Jun [c], M. Kaya [p], J. Kilmer [e], V.T. Kim [k], L.M. Kochenda [k], K. Königsmann [i,10], I. Konorov [i,11], A.P. Kozhevnikov [f], A.G. Krivshich [k], M.A. Kubantsev [h], V.P. Kubarovsky [f], A.I. Kulyavtsev [c,13], N.P. Kuropatkin [k], V.F. Kurshetsov [f], A. Kushnirenko [c], S. Kwan [e], J. Lach [e], A. Lamberto [t], L.G. Landsberg [f], I. Larin [h], E.M. Leikin [j], Li Yunshan [g], M. Luksys [n], T. Lungov [s,14], V.P. Maleev [k], D. Mao [c,13], Mao Chensheng [g], Mao Zhenlin [g], S. Masciocchi [i,12], P. Mathew [c,15], M. Mattson [c], V. Matveev [h], E. McCliment [p], M.A. Moinester [ℓ], V.V. Molchanov [f], A. Morelos [m], K.D. Nelson [p,16], A.V. Nemitkin [j], P.V. Neoustroev [k], C. Newsom [p], A.P. Nilov [h], S.B. Nurushev [f], A. Ocherashvili [ℓ], Y. Onel [p], E. Ozel [p], S. Ozkorucuklu [p], A. Penzo [t], S.V. Petrenko [f], P. Pogodin [p], B. Povh [i], M. Procario [c,17], V.A. Prutskoi [h], E. Ramberg [e], G.F. Rappazzo [t], B.V. Razmyslovich [k], V.I. Rud [j], J. Russ [c], Y. Scheglov [i], P. Schiavon [t], A.I. Sitnikov [h], D. Skow [e], V.J. Smith [o], M. Srivastava [s], V. Steiner [ℓ], V. Stepanov [k], L. Stutte [e], M. Svoiski [k], N.K. Terentyev [k,c], G.P. Thomas [a], L.N. Uvarov [k], A.N. Vasiliev [f], D.V. Vavilov [f], V.S. Verebryusov [h], V.A. Victorov [f], V.E. Vishnyakov [h], A.A. Vorobyov [k], J. You [c,e],

Zhao Wenheng [g], Zheng Shuchen [g], R. Zukanovich-Funchal [s]

[a] *Ball State University, Muncie, IN 47306, U.S.A.*

[b] *Bogazici University, Bebek 80815 Istanbul, Turkey*

[c] *Carnegie-Mellon University, Pittsburgh, PA 15213, U.S.A.*

[d] *Centro Brasiliero de Pesquisas Físicas, Rio de Janeiro, Brazil*

[e] *Fermilab, Batavia, IL 60510, U.S.A.*

[f] *Institute for High Energy Physics, Protvino, Russia*

[g] *Institute of High Energy Physics, Beijing, P.R. China*

[h] *Institute of Theoretical and Experimental Physics, Moscow, Russia*

[i] *Max-Planck-Institut für Kernphysik, 69117 Heidelberg, Germany*

[j] *Moscow State University, Moscow, Russia*

[k] *Petersburg Nuclear Physics Institute, St. Petersburg, Russia*

[ℓ] *Tel Aviv University, 69978 Ramat Aviv, Israel*

[m] *Universidad Autónoma de San Luis Potosí, San Luis Potosí, Mexico*

[n] *Universidade Federal da Paraíba, Paraíba, Brazil*

[o] *University of Bristol, Bristol BS8 1TL, United Kingdom*

[p] *University of Iowa, Iowa City, IA 52242, U.S.A.*

[q] *University of Michigan-Flint, Flint, MI 48502, U.S.A.*

[r] *University of Rome "La Sapienza" and INFN, Rome, Italy*

[s] *University of São Paulo, São Paulo, Brazil*

[t] *University of Trieste and INFN, Trieste, Italy*

Abstract

The Σ^- mean squared charge radius has been measured in the space-like Q^2 range 0.035–0.105 GeV$^2/c^2$ by elastic scattering of a Σ^- beam off atomic electrons. The measurement was performed with the SELEX (E781) spectrometer using the Fermilab hyperon beam at a mean energy of 610 GeV/c.

We obtain $\langle r^2_{ch} \rangle_{\Sigma^-} = (0.61 \pm 0.12\,(stat.) \pm 0.09\,(syst.))$ fm^2. The proton and π^- charge radii were measured as well and are consistent with results of other experiments. Our result agrees with the recently measured strong interaction radius of the Σ^-.

Key words: Electromagnetic form factors, elastic scattering, hadron-induced elastic scattering at high energy, hyperons, electron-Σ^- elastic scattering, Σ^- form factor, Σ^- charge radius, hadron strong and electromagnetic radii
PACS: 13.40.Gp, 13.60.Fz, 13.85.Dz, 14.20.Jn

1 Introduction

The systematic measurement of the static properties of hadrons has led to a better understanding of their fundamental structure. However, their finite size – a consequence of the confinement of quarks inside a spatial volume – has not been thoroughly explored. Sizes of hadrons may be probed by their strong and electromagnetic interactions. Most commonly the electromagnetic charge radius is measured in elastic electron-hadron scattering. For unstable hadrons the inverse kinematics can be applied using a suitable hadronic beam. So far, electromagnetic radii have been established only for the proton [1], neutron [2], π^- [3], and K^- [4]. The difference between the pion and the kaon radius indicates a dependence on the strangeness content. A systematic study of the radii of hyperons with different strangeness will therefore enhance our understanding of the relative sizes of hadrons as bound quark systems. Theoretical predictions for the Σ^- charge radius have been divergent [5]. The most recent efforts suggest $\langle r^2_{ch} \rangle_{\Sigma^-} = (0.67 \pm 0.03)\,\mathrm{fm}^2$ [6] on the one hand and $\langle r^2_{ch} \rangle_{\Sigma^-} = (0.54 \pm 0.09)\,\mathrm{fm}^2$ [7] on the other. The feasibility of probing the Σ^- radius by inverse electron scattering has been demonstrated at CERN [8]. We present here the first high-statistics measurement of the Σ^- charge radius.

[1] Corresponding author. *E-mail:* ivo@slac.stanford.edu
[2] Now at Imperial College, London SW7 2BZ, U.K.
[3] Present address: Boston Consulting Group, München, Germany
[4] Present address: Siemens Medizintechnik, Erlangen, Germany
[5] Present address: Deutsche Bank AG, Eschborn, Germany
[6] deceased
[7] Present address: Infineon Technologies AG, München, Germany
[8] Now at University of Karlsruhe, Karlsruhe, Germany
[9] Now at Instituto de Física da Universidade Estadual de Campinas, UNICAMP, SP, Brazil
[10] Now at Universität Freiburg, Freiburg, Germany
[11] Now at Physik-Department, Technische Universität München, Garching, Germany
[12] Now at Max-Planck-Institut für Physik, München, Germany
[13] Present address: Lucent Technologies, Naperville, IL
[14] Now at Instituto de Física Teórica da Universidade Estadual Paulista, São Paulo, Brazil
[15] Present address: SPSS Inc., Chicago, IL
[16] Now at University of Alabama at Birmingham, Birmingham, AL 35294
[17] Present address: DOE, Germantown, MD

2 The E781/SELEX Experiment

The primary objective of SELEX is the study of charm hadroproduction and spectroscopy of charm baryons in the forward hemisphere. The experiment was built as a 3-stage magnetic spectrometer as shown in Fig. 1. Here we only describe those features of the apparatus which are relevant to hadron-electron scattering.

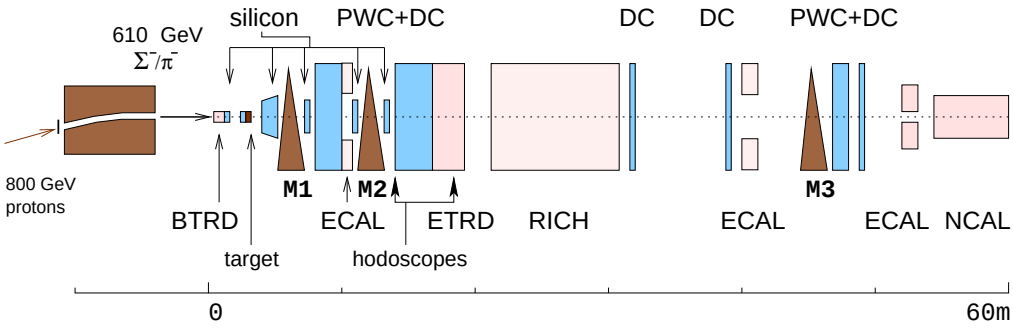

Fig. 1. Schematic layout of the SELEX apparatus [9]. The spectrometer stages are defined by the three magnets stylized as triangles. Transverse dimensions are not to scale.

The 800 GeV/c proton beam from the Fermilab Tevatron was steered onto a Be target to produce a beam consisting of equal numbers of Σ^- and π^- at 610 GeV/c mean momentum. The hyperon beam had a momentum spread of $\Delta p/p = \pm 8\%$. Other constituents were 1 % Ξ^- and less than 0.1 % other particles. The magnet polarity could be reversed to provide a 540 GeV/c beam containing 94 % protons and 3 % each of π^+ and Σ^+. A transition radiation detector (BTRD) separated the baryonic from the mesonic beam components. Interactions took place in a target stack of two Cu and three C foils adding up to 4.2 % of an interaction length for protons. The first two magnets (M1, M2) implemented momentum cuts of 2.5 GeV/c and 15 GeV/c, respectively. Downstream of the second magnet a second transition radiation detector (ETRD) identified scattered electrons. Each stage of the spectrometer was equipped with a lead glass calorimeter (ECAL). Tracking information was provided by a combination of silicon microstrip detectors, proportional chambers (PWC), and drift chambers (DC).

Candidates for elastic scattering events were selected by a scintillator-based trigger requiring two charged particles in the M2 spectrometer both of which originated in the target area. The total multiplicity signal directly downstream of the targets was combined with the charge and multiplicity information from the hodoscope after magnet M2. The total charge was required to correspond to one beam particle plus one electron. An online filter refined this selection by checking for the same topology using particle tracks reconstructed in the

M2 spectrometer.

3 Kinematics

The differential cross section of the elastic scattering of a spin 1/2 baryon (mass M) off an electron (mass m) can be approximated by the relation ($\hbar = c = 1$)[10]

$$\frac{d\sigma}{dQ^2} = \frac{4\pi\alpha^2}{Q^4}\left(1 - \frac{Q^2}{Q^2_{max}}\right) F^2(Q^2) \tag{1}$$

up to corrections of the order $m^2/(s - M^2)$. Here, s denotes the center of mass energy and Q^2 the four momentum transfer from the hadron to the electron. Q^2 has a kinematically allowed maximum value which depends on the beam momentum. For instance, Q^2_{max} is 0.2 GeV^2/c^2 for 610 GeV/c Σ^-. For $m \ll M$ the squared form factor can be written as a combination of the electric and magnetic form factors $G_E(Q^2)$ and $G_M(Q^2)$:

$$F^2(Q^2) = \frac{G_E^2 + (Q^2/4M^2)G_M^2}{1 + (Q^2/4M^2)} + \frac{Q^4}{2(4M^2E^2 - (2ME + M^2)Q^2)}G_M^2, \tag{2}$$

with E being the beam energy in the laboratory frame. These form factors are normalized to the charge $G_E(0) = Z$ and the magnetic moment $G_M(0) = \mu$ of the baryon. The mean squared charge radius is defined by the relation

$$\langle r^2_{ch}\rangle = \frac{-6}{G_E(0)}\left.\frac{dG_E}{dQ^2}\right|_{Q^2=0}. \tag{3}$$

At low momentum transfers $Q^2 \leq 0.1\,\mathrm{GeV}^2/c^2$, both electric and magnetic form factors of the Σ^- can be parameterized by the dipole approximation:

$$\frac{G_E(Q^2)}{G_E(0)} = \frac{G_M(Q^2)}{G_M(0)} = D(Q^2) = \left(1 + \frac{\langle r^2_{ch}\rangle Q^2}{12}\right)^{-2}. \tag{4}$$

A fit of equation (1) to the shape of the measured Q^2 distribution provides the information on $\langle r^2_{ch}\rangle$ by means of equation (4).

4 Analysis and Results

Out of 77 million triggers with a Σ^- a sample of 5010 Σ^--electron scattering events was extracted as follows: The events containing one electron were selected and the particle trajectories combined to check if they formed vertices inside the target material. The event was accepted if it contained exactly three tracks forming one vertex consisting of the beam track, the electron candidate, and the scattered hadron candidate.

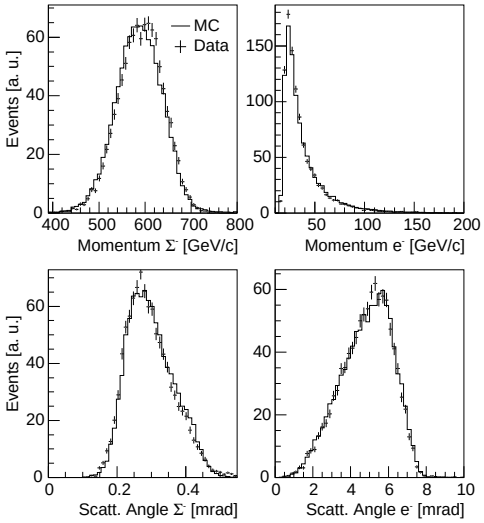

Fig. 2. Comparison of the elastic scattering observables in data and simulation.

At a given beam energy, momenta and scattering angles of the outgoing electron and hadron (Fig. 2) provide four observables to determine the four-momentum transfer from hadron to electron (Fig. 3a). As the measurement is overdetermined, the electron momentum could be ignored, thus avoiding sizable radiative corrections. This is an important advantage of the reversed method since in experiments with an electron beam the corrections for Bremsstrahlung have a direct influence on the result. The remaining radiative corrections to the Q^2 spectrum due to initial Bremsstrahlung loss are small, and show a variation of less than 0.2% in the Q^2 region used in this analysis. The momentum transfer was fitted to the remaining three observables. In the last stage of the event selection, both scattering angles and the momentum loss of the hadron were required to satisfy the constraints imposed by elastic kinematics.

A full GEANT [11] simulation of detector, trigger, reconstruction, and analysis was performed (Fig. 2), which yielded the correction for acceptance effects of the experimental setup (Fig. 3b). At $Q^2 < 0.03\,\mathrm{GeV}^2/c^2$ the electron is driven out of the geometric acceptance as a result of the M2 magnetic field. For $Q^2 > 0.11\,\mathrm{GeV}^2/c^2$ the electron is likely to hit the central sections of

the hodoscopes together with the hadron, not producing a trigger. In the remaining Q^2 range the acceptance has only minor variations reflecting the individual efficiencies of hodoscope segments.

To eliminate kinematic effects from varying beam energy, the measured differential cross section was weighted with the Mott scattering cross section, accounting for the magnetic moment of the hadron. This yields the squared dipole form factor $D^2(Q^2)$ which in turn provides $\langle r_{ch}^2 \rangle$(Eqn. (4); Fig. 3c). This method is more sensitive to $\langle r_{ch}^2 \rangle$ than an unbinned maximum likelihood fit of the Q^2 distribution even though it adds binning effects to the systematic uncertainty [12]. The fit of $D^2(Q^2)$ was restricted to the Q^2 region of minimal systematic error between 0.035 GeV$^2/c^2$ and 0.105 GeV$^2/c^2$.

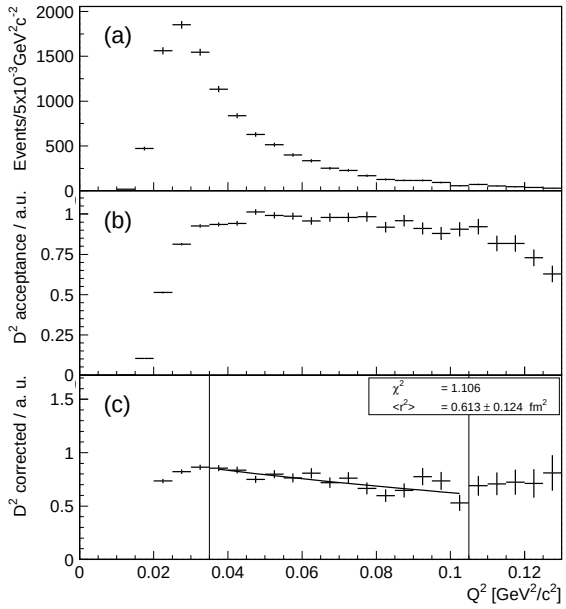

Fig. 3. (a) Q^2 distribution of the final event sample. (b) Acceptance function applied to a constant dipole term $D^2(Q^2)$. (c) Fit to $D^2(Q^2)$ extracted from data corrected for acceptance. Vertical lines indicate boundaries of fit. D^2 is given in arbitrary units, statistical error only.

The systematic errors in $\langle r_{ch}^2 \rangle$ introduced by cuts on kinematic variables (χ^2 of the vertex fit, sum of momenta, scattering angles of electron and hadron) were estimated by varying one cut at a time by $\pm 1\sigma$ of its resolution. Systematic dependence of the result on the fit boundaries was studied over the full Q^2 range. The boundaries were selected so as to minimize this dependence, and the remaining contribution to the systematic error determined by varying them by $\pm 1\sigma$ of the Q^2 resolution. The contribution of histogram binning effects was evaluated by systematically changing the bin width.

The total systematic error (table 1) is dominated by the choice of cuts on kinematic variables on one hand and the choice of fit boundaries on the other.

Table 1
Contributions to the systematic error of $\langle r^2_{ch} \rangle_{\Sigma^-}$ (in fm^2).

Cuts on kinematic variables	0.04
Choice of fit boundaries	0.04
Histogram binning effects	0.03
Beam contamination	0.01

The number of events in the final selection corresponds to 4 % of elastic Σ^--electron events expected in this interval. The efficiency of this measurement was mainly limited by trigger (23 %) and reconstruction efficiencies (21 %). Background from Ξ^--electron scattering was estimated to be present in far less than one percent of the final event sample. A different class of background can be caused by events of the form $\Sigma^- \ \pi^0 \rightarrow \Sigma^- \ \gamma e^- e^+$. If the positron is not detected due to early absorption or tracking inefficiency, the event topology can appear to be similar to Σ^--electron scattering. Events of this kind have been observed in early SELEX data where the interaction counter had been mistuned. The invariant mass of reconstructed electrons and photons in the ECAL shows no evidence of such events in the final event sample.

Our result for the mean squared Σ^- electromagnetic radius is

$$\langle r^2_{ch} \rangle_{\Sigma^-} \ = \ (0.61 \ \pm 0.12 \, (stat.) \ \pm 0.09 \, (syst.)) \ \text{fm}^2.$$

In order to facilitate an interpretation of this result free of any systematics introduced by the experimental setup, the mean squared electromagnetic proton radius was measured as well. Using the same procedure as described for the Σ^- analysis [13] we obtain

$$\langle r^2_{ch} \rangle_p \ = \ (0.69 \ \pm 0.06 \, (stat.) \ \pm 0.06 \, (syst.)) \ \text{fm}^2,$$

which is in good agreement with results from elastic *ep* scattering experiments (overall $\langle r^2_{ch} \rangle_p = 0.77 \pm 0.03$ fm^2 [1]. Ref. [14] finds $\langle r^2_{ch} \rangle_p = 0.67 \pm 0.02$ fm^2 from data in a Q^2 range that overlaps well with ours). In addition we have determined the mean squared π^- charge radius from SELEX data assuming a monopole form factor [15]. Our result,

$$\langle r^2_{ch} \rangle_{\pi^-} \ = \ (0.42 \ \pm 0.06 \, (stat.) \ \pm 0.08 \, (syst.)) \ \text{fm}^2,$$

is consistent with the results of other experiments [3].

5 Discussion and Conclusion

To put our results in perspective, we compare the electromagnetic charge radii to radii derived from total hadron-proton cross sections (strong interaction radii [5], Fig. 4). The latter have been normalized to the mean squared charge radius of the proton as measured by SELEX at $\sqrt{s} = 34$ GeV and the total pp cross section [16] interpolated to this energy. Both the Σ^- and π^- squared strong interaction radii are calculated from total cross sections measured by SELEX [17] as well. The mean squared radii of the proton, Σ^-, and π^- were determined using identical experimental setup, reconstruction, and analysis procedure. We therefore expect these particular results to be free of systematic error in respect to each other, and only statistical errors are displayed in Fig. 4.

For reference we added the squared K^- charge radius [4] as well as the squared strong interaction radii of K^- and Ξ^- to Fig. 4. The K^- strong interaction radius was extrapolated to SELEX energy using the Particle Data Group's parameterization of the K^-p total cross section [16]. For the Ξ^- we used the radius determined at $\sqrt{s} = 16$ GeV [18]. It was not scaled to SELEX energy for lack of Ξ^-p cross section data.

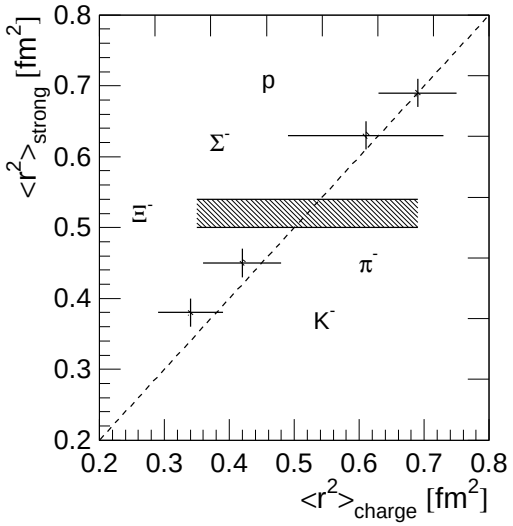

Fig. 4. Comparison of strong and electromagnetic mean squared radii for proton, Σ^-, and π^- from SELEX data for which only statistical errors are displayed. Equality of strong interaction and charge radius is indicated by the dashed line. The radii of K^- and Ξ^- from other experiments are included for reference (see also table 2).

We conclude that our results for the mean squared electromagnetic charge radii of proton, Σ^-, and π^- agree with the values of their mean squared strong interaction radii. They also confirm the charge radii reported by previous experiments. The Σ^- charge radius is comparable within errors to that of the proton, yet compatible with a smaller value as suggested by the trend

indicated by strong interaction radii: the results imply a ratio $\langle r^2_{ch}\rangle_p / \langle r^2_{ch}\rangle_{\Sigma^-} = 1.13 \pm 0.24$.

Table 2
Mean squared electromagnetic and strong interaction radii shown in Fig. 4.

	Electromagnetic	Strong interaction
	$\langle r^2_{ch}\rangle$[fm^2]	$\langle r^2_{st}\rangle$ [fm^2]
p	0.69 ± 0.06	0.69 ± 0.02
Σ^-	0.61 ± 0.12	0.63 ± 0.02
π^-	0.42 ± 0.06	0.45 ± 0.02
K^-	0.34 ± 0.05	0.38 ± 0.02
Ξ^-		0.52 ± 0.02

Our result for the Σ^- is at this point the best direct measurement of the charge radius of a charged baryon other than the proton. It covers an unprecedented range of squared momentum transfer Q^2 between Σ^- and electron. With this experiment we have proven that it is possible to measure baryon charge radii in inverse kinematics with high precision. Due to the Q^{-4} behavior of the differential cross section the accuracy of the final result is limited by the low statistics towards higher Q^2.

In a dedicated experiment it would be possible to extend trigger and reconstruction to both lower and higher Q^2, allowing for increased statistics and better control of the systematics. By using very finely segmented hodoscopes, for example, one could trigger on hadron-electron pairs of very small common angle, extending the acceptance to higher Q^2. Since this relaxes the requirements for hadron-electron separation one could at the same time reduce the magnetic field strength downstream of the targets to have access to lower Q^2 as well.

Acknowledgements

The authors are indebted to the staff of Fermi National Accelerator Laboratory and for invaluable technical support from the staffs of collaborating institutions, especially F. Pearsall, D. Northacker, and J. Zimmer. This project was supported in part by the Bundesministerium für Bildung, Wissenschaft, Forschung und Technologie, Consejo Nacional de Ciencia y Tecnología (CONACyT), the Conselho Nacional de Desenvolvimento Científico e Tecnológico, the Fondo de Apoyo a la Investigación (UASLP), the Fundação de Amparo à Pequisa do Estado de São Paulo (FAPESP), the Israel Science Foundation founded by the Israel Academy of Sciences and Humanities,

Istituto Nazionale di Fisica Nucleare (INFN), the International Science Foundation (ISF), the National Science Foundation (Phy#9602178), NATO (grant CR6.941058-1360/94), the Russian Academy of Science, the Russian Ministry of Science and Technology, the Turkish Scientific and Technological Research Board (TÜBİTAK), the U.S. Department of Energy (DOE grant DE-FG02-91ER40664), and the U.S.-Israel Binational Science Foundation (BSF).

References

[1] R. Rosenfelder, Phys Lett B479, 381 (2000), and references therein.

[2] S. Kopecky *et al.*, Phys Rev Lett 74, 2427 (1995).

[3] S. Amendolia *et al.*, Nucl Phys B277, 186 (1986).

[4] S. Amendolia *et al.*, Phys Lett B178, 435 (1986).

[5] B. Povh and J. Hüfner, Phys Lett B245, 653 (1990), and references therein.

[6] B. Kubis and U.G. Meissner, Eur. Phys. J. C18, 747 (2001).

[7] E.J. Hackett-Jones, D.B. Leinweber, and A.W. Thomas, Phys Lett B494, 89 (2000)

[8] M. Adamovich *et al.*, Eur. Phys. J. C8, 59 (1999).

[9] I. Eschrich in: *Proceedings of the 8th International Conference on the Structure of Baryons*, D. W. Menze and B. Metsch, eds., World Scientific Publishing Co. (1999), `hep-ex/9811003`.

[10] G. Källén, *Elementary particle physics*, Addison-Wesley Publishing Company (1964). Also see S.S. Gershtein *et al.*, IHEP preprint 89-88 (1989, in Russian).

[11] *GEANT - Detector Description and Simulation Tool*, CERN Program Library Long Writeup W5013 (1994).

[12] J. Simon, Ph.D. thesis, MPI f. Kernphysik/ Univ. Heidelberg (2000, in German); I. Eschrich, Ph.D. thesis, MPI f. Kernphysik/ Univ. Heidelberg (1998), MPIH-V22-1998. Both theses are available at `http://fn781a.fnal.gov`.

[13] H. Krüger, Ph.D. thesis, MPI f. Kernphysik/ Univ. Heidelberg (1999, in German). Available at `http://fn781a.fnal.gov`.

[14] J.J. Murphy *et al.*, Phys Rev C9, 2125 (1974).

[15] G. Dirkes, Diplomarbeit, MPI f. Kernphysik/ Univ. Heidelberg (1999, in German); K. Vorwalter, Ph.D. thesis, MPI f. Kernphysik/ Univ. Heidelberg (1998), MPIH-V23-1998; I. Giller, M.Sc. thesis, Tel Aviv University (1999). All of the above are available at `http://fn781a.fnal.gov`.

[16] D.E. Groom *et al.*, Eur. Phys. J. C15, 1 (2000).

[17] U. Dersch *et al.*, Nucl. Phys. C579, 277 (2000).

[18] B. Povh and J. Hüfner, Phys Rev Lett 58, 1612 (1987).